

Diagnostics of Eccentricities and Bar/End-Ring Connector Breakages in Polyphase Induction Motors Through a Combination of Time-Series Data Mining and Time-Stepping Coupled FE–State-Space Techniques

John F. Bangura, *Member, IEEE*, Richard J. Povinelli, *Senior Member, IEEE*, Nabeel A. O. Demerdash, *Fellow, IEEE*, and Ronald H. Brown, *Member, IEEE*

Abstract—This paper develops the foundations of a technique for detection and categorization of dynamic/static eccentricities and bar/end-ring connector breakages in squirrel-cage induction motors that is not based on the traditional Fourier transform frequency-domain spectral analysis concepts. Hence, this approach can distinguish between the “fault signatures” of each of the following faults: eccentricities, broken bars, and broken end-ring connectors in such induction motors. Furthermore, the techniques presented here can extensively and economically predict and characterize faults from the induction machine adjustable-speed drive design data without the need to have had actual fault data from field experience. This is done through the development of dual-track studies of fault simulations and, hence, simulated fault signature data. These studies are performed using our proven Time-Stepping Coupled Finite-Element–State-Space method to generate fault case performance data, which contain phase current waveforms and time-domain torque profiles. Then, from this data, the fault cases are classified by their inherent characteristics, so-called “signatures” or “fingerprints.” These fault signatures are extracted or “mined” here from the fault case data using our novel Time-Series Data Mining technique. The dual track of generating fault data and mining fault signatures was tested here on dynamic and static eccentricities of 10% and 30% of air-gap height as well as cases of one, three, six, and nine broken bars and three, six, and nine broken end-ring connectors. These cases were studied for proof of principle in a 208-V 60-Hz four-pole 1.2-hp squirrel-cage three-phase induction motor. The paper presents faulty and healthy performance characteristics and their corresponding so-called phase space diagnoses that show distinct fault signatures of each of the above-mentioned motor faults.

Index Terms—Artificial intelligence, data mining, diagnostics through current waveforms, dynamical systems analysis, electric drives, fault diagnosis, induction motors, state-space methods, time series, time-stepping finite elements.

Paper IPCSD 03–030, presented at the 2001 Industry Applications Society Annual Meeting, Chicago, IL, September 30–October 5, and approved for publication in the IEEE TRANSACTIONS ON INDUSTRY APPLICATIONS by the Electric Machines Committee of the IEEE Industry Applications Society. Manuscript submitted for review October 15, 2001 and released for publication April 25, 2003.

J. F. Bangura is with Black & Decker, Towson, MD 21286 USA (e-mail: John.Bangura@bdk.com).

R. J. Povinelli, N. A. O. Demerdash, and R. H. Brown are with the Department of Electrical and Computer Engineering, Marquette, University, Milwaukee, WI 53233 USA (e-mail: Richard.Povinelli@Marquette.edu; Nabeel.Demerdash@Marquette.edu; Ron.Brown@Marquette.edu).

Digital Object Identifier 10.1109/TIA.2003.814582

I. INTRODUCTION

THREE-PHASE induction motors are presently in common use in a majority of electronically controlled ac adjustable/variable-speed drives. During the past 20 years, there have been continuing efforts at studying and diagnosing faults in ac motor drives. A large number of these studies are cited in a major bibliographical paper under the aegis of the Electric Machinery Committee of the IEEE Power Engineering Society, which is authored by Benbouzid [1]. The bulk of fault diagnostics/detection and monitoring investigations can largely be divided into three categories.

The first category comprises work that centered on traditional lumped-parameter modeling and analysis of faulty motor performance, and case-history studies of actual motor faults in stators, rotors and bearings, as well as field experience and practical engineering insights into the causes and effects of these faults (see [2]–[5]).

The second category comprises investigations that centered upon “online” motor condition monitoring and fault diagnostics using the motor terminal current and voltage waveforms, while applying traditional Fourier transform spectral analysis techniques to these waveforms in actual case-study field experience. Some of these works included applications of neural network and other artificial intelligence (AI) methods to these spectral analyses results (see [6]–[17]).

The third category consists of a small number of investigations in which the method of finite-element analysis of electric motor performance was enlisted in fault diagnostic studies, these works were rather limited in scope (see [18]–[20]).

Although the above brief summary indicates the existence of a large body of work and research on fault monitoring and diagnostics in motor drive systems, it also indicates that much to be desired is yet to be accomplished. In particular, there are two main problems, which we begin to address in this paper. The first is a modeling algorithm that addresses the lack of comprehensive field fault databases. The second is an algorithm that addresses the difficulty in distinguishing between degrees of faults.

Our approach to the problem of diagnosing faults in induction motor adjustable-speed drives (IMASDs) is new and unique.

First, knowing the design details of a motor-drive system, we can generate data for a plethora of fault conditions by simulations obtained from the experimentally verified Time-Stepping Coupled Finite-Element-State-Space (TSCFE-SS) method [21]–[25]. This is without the need to encounter and acquire data for such faults in actual field experience with IMASDs. Second, using Time-Series Data Mining (TSDM) [26]–[28], hidden patterns and nuances of differences between healthy performance signatures and various fault signatures can be identified. These fault signatures reveal the severity (percentage of air-gap height) of dynamic and static eccentricities, the severity (approximate number) of broken squirrel-cage bars, and the severity (approximate number) of broken end-ring connectors. That is, this approach automatically and efficiently identifies and makes use of the data of these fault signatures in fault diagnostics.

The faulty operations being studied here include: 10% and 30% degrees of static and dynamic eccentricities, as well as one, three, six, and nine broken bars in addition to three, six, and nine broken end-ring connectors [23], [24]. The advantage of this dual track method lies in its rigor in predicting effects of motor faults on performance. The second portion of this dual track identifies and extracts hidden patterns and nuances that are characteristic and predictive of specific faults through data mining of the fault signatures.

Accordingly, this paper presents the development of a comprehensive set of algorithms for fault simulation, and fault identification/diagnosis in IMASDs. Specifically, we expand the number and type of faults by studying motor shaft eccentricities and the difficult case of a single broken bar in a side-by-side comparison with other squirrel-cage breakages (broken bars and broken connectors). We have developed a new, more sophisticated algorithm for differentiating these new types of faults from those presented in an earlier paper [28].

II. TSCFE-SS METHOD

The TSCFE-SS technique [21]–[25] computes on a time instant-by-instant basis (time profiles/waveforms) the input phase and line currents, voltages, developed power, and torque of a motor as functions of the particular magnetic circuit, winding layouts, and materials as well as inverter (power conditioner) operating conditions. Computations include the full effects of interaction of machine space harmonics with time-domain harmonics due to modern fast electronic switching on overall motor-controller/drive performance [25], [29]. Thus, the TSCFE-SS algorithms can also be used in parametric design studies.

The TSCFE-SS aspect fully incorporates the nonlinear effects of magnetic saturation in the machine and makes full use of the natural machine winding's frame of reference (for details see [21]–[25]). Also, see Fig. 1 for the functional flowchart block diagram, which summarizes the essence of this approach. Hence, again this assures inclusion of all significant space harmonics due to the physical design and nonlinear nature of the motor's magnetic circuit, as well as the time harmonics generated from the inverter switching in the motor-drive modeling and simulations. Accordingly, the simulated fault signatures are derived

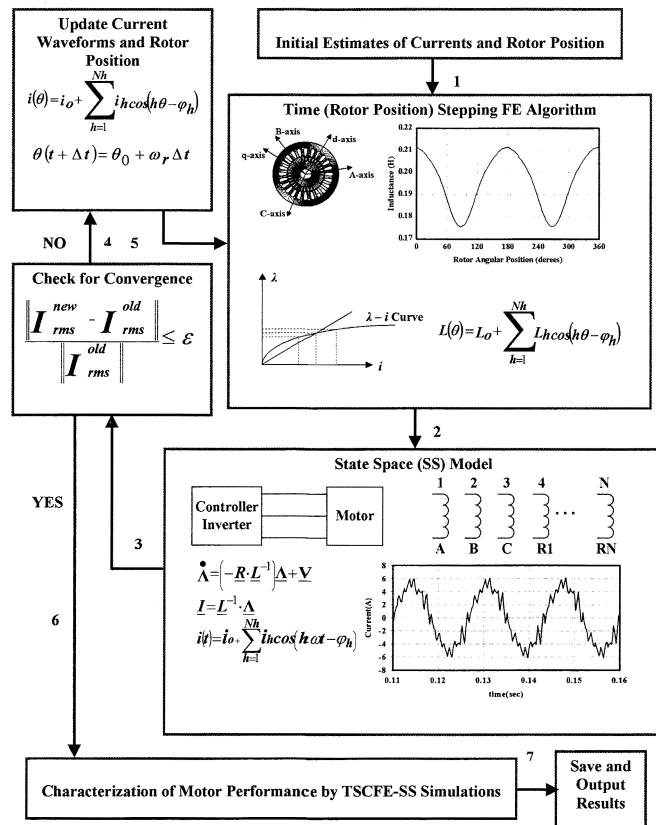


Fig. 1. Functional block diagram/flowchart of the TSCFE-SS method.

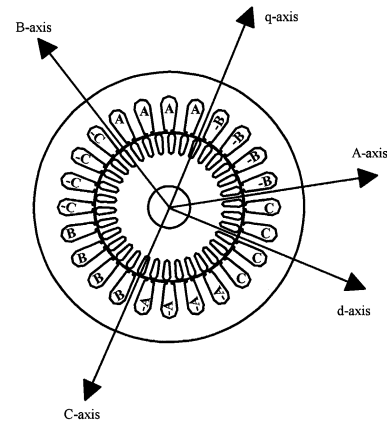


Fig. 2. Motor cross section.

from time-domain phase current and voltage waveforms, and from simulated instantaneous torque profiles that rigorously incorporate the motors' design characteristics.

The state model for the 1.2 hp motor, the cross section of which is given in Fig. 2, was derived from generalized machine theory using the natural *abc* frame of reference, and the inverter and machine models were integrated. The state variables in this model are the *a*, *b*, and *c* armature windings' flux linkages as well as the 34 flux linkages of the 34 squirrel-cage loops under healthy motor conditions (see the motor's cross section of Fig. 2 and the developed squirrel-cage loop diagram of Fig. 3). Again, for details, [21]–[25] should be consulted. To represent bar breakages and end-ring connector breakages the

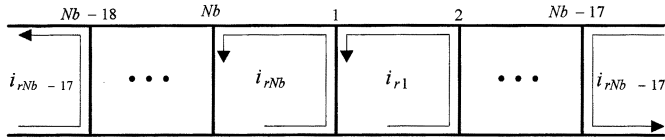


Fig. 3. Schematic representation of the modeling of a healthy cage.

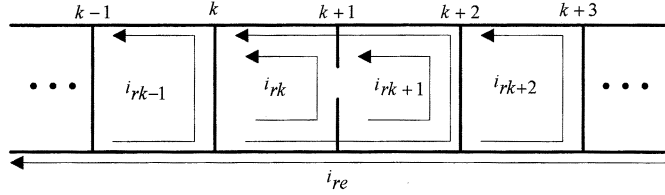


Fig. 4. Schematic representation of the modeling of a broken rotor bar.

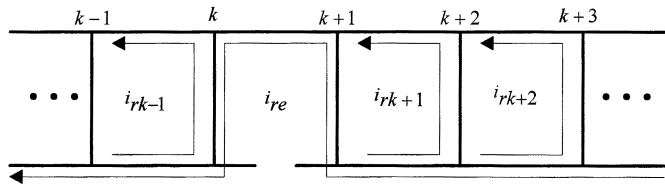


Fig. 5. Schematic representation of the modeling of a broken end-ring connector.

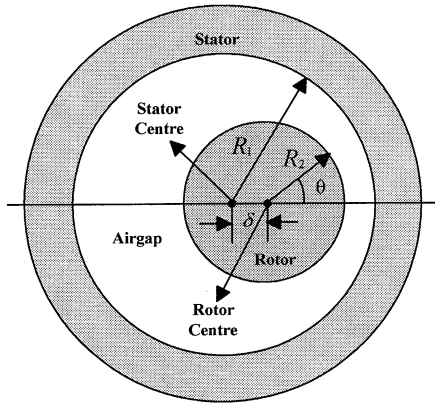


Fig. 6. Schematic representation of air-gap eccentricity.

squirrel-cage loops need to be disturbed according to patterns such as shown in Figs. 4 and 5, respectively. See [23] for further details.

As for the cases of static and dynamic eccentricities, those were modeled by disturbing the rotor's location and consequently its FE grid's location as shown schematically in Fig. 6. The schematic in Fig. 6 can represent the static and dynamic eccentricities depending on which of the two points separated by the distance, δ , are made to be the axis of rotor rotation (for details [24] should be consulted further). In essence, in static eccentricity the air gap takes the shape of a stationary crescent-like pattern, while in dynamic eccentricity the air gap takes the shape of a continuously modulated revolving crescent.

The TSCFE-SS model yields the steady-state time-domain profiles of the change in all winding (loop) inductances under actual time-varying saturation conditions, and all the steady-state time-domain profiles/waveforms of the developed machine torque and all the 37 winding currents (three are the a , b , and

c stator armature currents, the remainder are the squirrel-cage loop currents whose number is 34 or less depending on the pattern of bar/connector breakages being simulated).

III. TSDM METHOD

The TSDM method, the second track of the dual-track approach, addresses the problem of differentiating various types and degrees of motor drive faults. The TSDM method reveals hidden patterns in time series data (current and voltage waveforms as well as time-domain torque profiles). A clear distinction is shown here between the various faulty and healthy modes of motor operation. Our approach provides a definite new advantage over frequency-spectrum Fourier transform techniques particularly used for fault diagnostics by earlier investigators [6]–[17].

A process called time-delay embedding [30] is used to transform the torque time series into a reconstructed state space, also called a phase space. Given the first difference torque time series $\Delta T = \{\Delta\tau(k), k = 2, \dots, N\}$, where $\Delta\tau = \tau(k) - \tau(k-1)$, k is a time index, and N is the number of observations, a two-dimensional phase space is created by plotting $\Delta\tau(k-10)$ on the x - y plane's abscissa and $\Delta\tau(k)$ on the ordinate. See Figs. 13–24 for examples of such phase spaces.

This approach is based soundly in dynamical systems theory. Takens showed that the time-delay embedding process is able to reconstruct a topologically identical state space to the original state space of the system [31]. Hence, the features that capture the similarities and differences of the reconstructed state space are capturing similarities and differences of the underlying state structure of the system. We exploit this theoretical relationship between the reconstructed state space and the original state space to distinguish motor drive faults.

The feature used for distinguishing between reconstructed phase spaces generated for different healthy and faulty modes of motor operation is the so-called radius of gyration [32] (which is used in this work as a fault identification parameter) around the center of mass of the points in the phase space, where each point in the phase space is given a unit mass. The radius of gyration r is calculated as follows [32]:

$$r = \sqrt{\frac{\sum_{k=1+l}^N d(k)^2}{N-l}} \quad (1)$$

where the distance $d(k)$ between the center of mass and the k th point in the phase space is

$$d(k)^2 = (x(k) - \mu_0)^2 + (x(k-l) - \mu_l)^2 \quad (2)$$

and μ_0 and μ_l , the centers of mass for their respective dimensions, are

$$\mu_m = \frac{\sum_{k=1+l+m}^{N-l+m} x(k)}{N-l}. \quad (3)$$

Additionally, l is the time lag of the phase space, N is the number of observations, and $x(k)$ is the time-series observation at time index k (see [30] for details of the time-delay embedding process). It should be pointed out that $d(k)$ is the distance of the k th phase-space "point" from the center of mass of the phase-space "points." Since we are using a two-dimensional

phase space, which is formed by plotting $x(k-l)$ on the x - y plane's abscissa and $x(k)$ on the ordinate, the square of the distance is calculated by summing the squares of the differences between the phase-space point's value in each dimension and its corresponding center of mass for that same dimension. The value μ_m is the center of mass for each phase-space dimension.

This radius of gyration feature is a sufficient first approximation of the phase space to allow distinguishing between the motor's healthy mode of operation and various squirrel-cage breakage faults being presented here. It is also sufficient to identify the degree of the eccentricity, e.g., it allows the differentiation between modes of operation of 10% and 30% degrees of eccentricities. However, we introduce here a second feature, which is required to differentiate between the dynamic and static eccentricities of the same degree. This second feature is the standard deviation σ of the radius of gyration, which is defined as follows:

$$\sigma = \sqrt{\frac{(N-l) \sum_{k=1+l}^N (d(k))^2 - \left(\sum_{k=1+l}^N d(k)\right)^2}{(N-l)(N-l-1)}}. \quad (4)$$

The algorithm for classifying the profiles is essentially a two-step process. The first step categorizes all broken bar, end-ring connector, and eccentricity faults. It also determines the number of broken bars, number of broken end-ring connectors, or the degree of the eccentricity. If required, the second step determines the type of eccentricity.

Given a motor's time-domain torque first difference as a time series (profile), and its corresponding reconstructed phase space, the algorithm, for determining the unknown operating mode of the motor from which the time-domain torque profile was sampled, is best described as follows.

Algorithm IDENTIFY MODE (R, r, Σ, σ)

Input. A set $R = \{r_1, r_2, \dots, r_n\}$ of the radii of gyration of the known operating modes, where n is the number of known operating modes. The radius of gyration for the unknown mode, r . A set $\Sigma = \{\sigma_1, \sigma_2, \dots, \sigma_m\}$ of the standard deviations of the radii of gyration for the eccentricity modes of operation, where m is the number of known eccentricity modes of operation. The standard deviation of the radius of gyration for the unknown mode, σ .

Output. The identified mode of operation.

- 1) $i = \text{index}(\min\{|r' - r| : r' \in R\})$. The index operator yields the "index of the mode" with the closest radius of gyration to the unknown mode.
- 2) **if** i is an index for an eccentricity mode of operation
- 3) **then** Form Σ' a subset of Σ with the standard deviations of the radii of gyration that have the same degree of eccentricity as the mode of operation corresponding to the index, i . For example if the index i corresponds to a 30% dynamic eccentricity, Σ' has as elements the standard deviations of the radii of gyration for the 30% static eccentricity and the 30% dynamic eccentricity.
- 4) $j = \text{index}(\min\{|\sigma' - \sigma| : \sigma' \in \Sigma'\})$. The index operator yields the "index of the mode" with the closest standard deviation of the radius of gyration

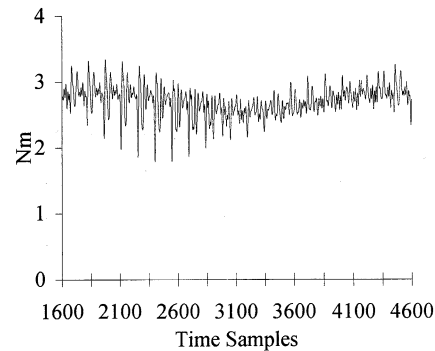


Fig. 7. Healthy motor torque profile.

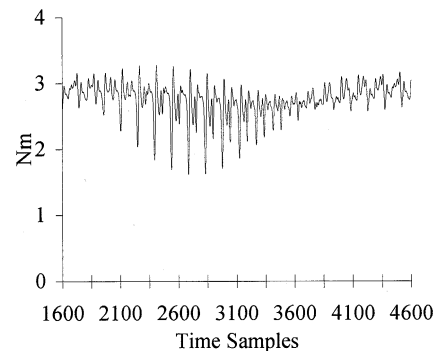


Fig. 8. 10% static eccentricity torque.

to the standard deviation of the radius of gyration of the unknown mode.

- 5) **return** the eccentricity mode of operation corresponding to the index j .
- 6) **else return** the mode of operation corresponding to the index i .

Since the diagnostic algorithm is expected to run online, as compared to the TSCFE-SS simulations, which are run offline, it is important to study both its computational and memory complexity. An analysis of the IDENTIFYMODE algorithm shows that it has both a $O(n)$ time and space complexity, where n is the number of torque samples, hence, the algorithm can be run in linear time. This is in comparison to any frequency based approach, which relies on the fast Fourier transform (FFT), which has a time complexity of $O(n \log n)$ and a space complexity of $O(n)$. Hence, from a processing complexity standpoint the IDENTIFYMODE algorithm is simpler than frequency-based methods and could easily be implemented in real time.

IV. TSCFE-SS SIMULATIONS

Simulations of the healthy cage case, the 10% and 30% static and dynamic eccentricity cases, as well as the one, three, six, and nine broken bar cases; the three, six, and nine broken end-ring connector cases were generated using our TSCFE-SS method. The resulting torque profiles for the simulation of the healthy rotor/cage case; the 10% and 30% static and dynamic eccentricity cases; and one broken bar case are given in Figs. 7–12, respectively. The torque profile simulations for the other cases were presented in [28]. The reconstructed phase

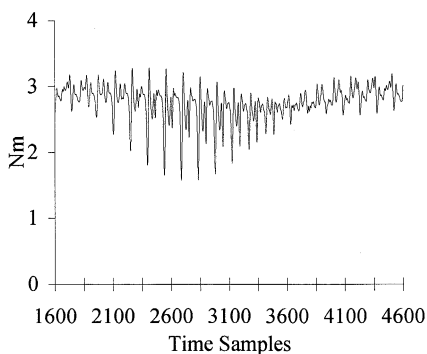


Fig. 9. 30% static eccentricity torque.

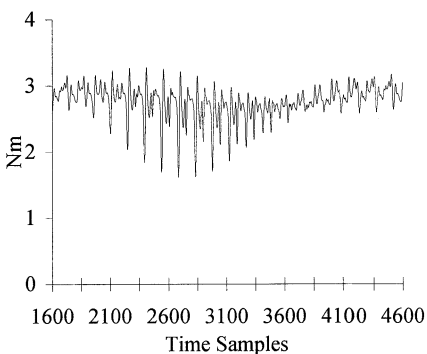


Fig. 10. 10% dynamic eccentricity torque.

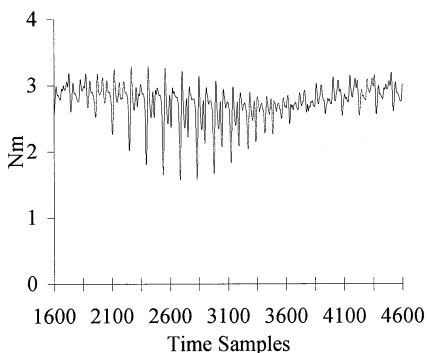


Fig. 11. 30% dynamic eccentricity torque.

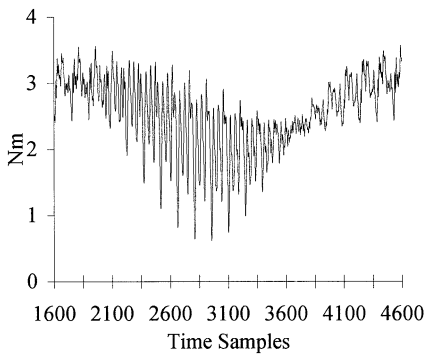


Fig. 12. One broken bar torque profile.

spaces of the torque first difference time series corresponding to the torque profile simulations for the healthy rotor/cage case and all the faulty rotor/cage cases mentioned above are illustrated in Figs. 13–24, respectively.

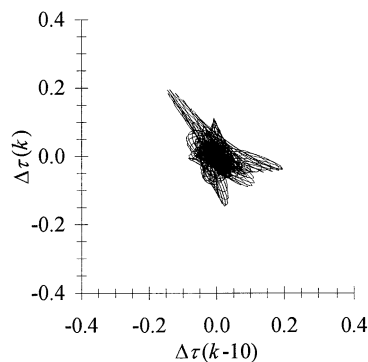


Fig. 13. Healthy motor torque first difference phase space.

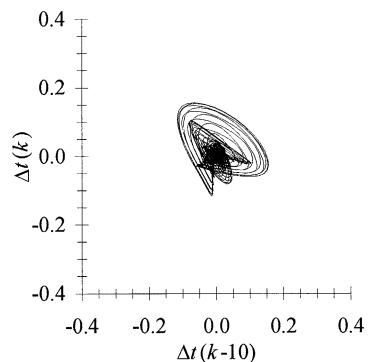


Fig. 14. 10% static eccentricity torque first difference phase space.

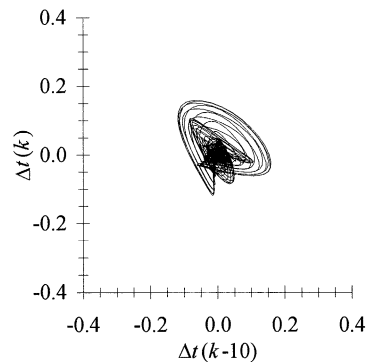


Fig. 15. 30% static eccentricity torque first difference phase space.

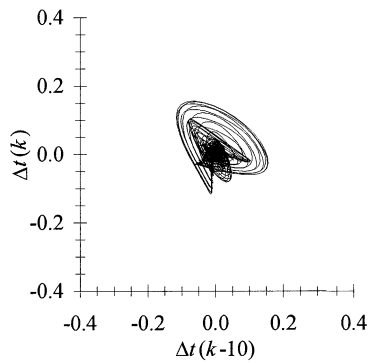


Fig. 16. 10% dynamic eccentricity torque first difference phase space.

Two concerns arise in relying on simulated datasets. The first is the reliability of the simulations. The first concern is addressed by comparing the resulting simulated profiles with the

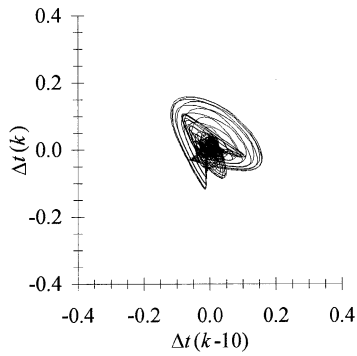


Fig. 17. 30% dynamic eccentricity torque first difference phase space.

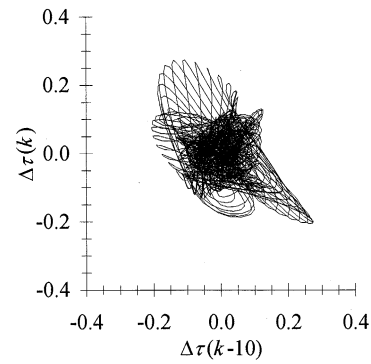


Fig. 21. Nine broken bars torque first difference phase-space.

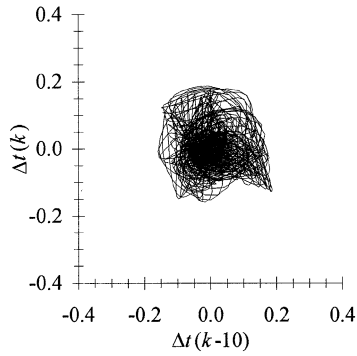


Fig. 18. One broken bar torque first difference phase space.

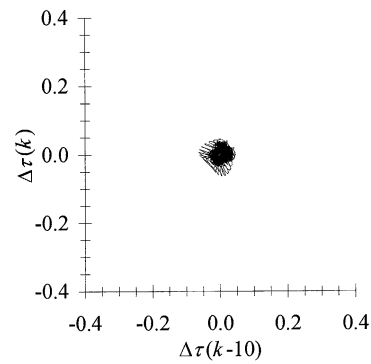


Fig. 22. Three broken connectors torque first difference phase space.

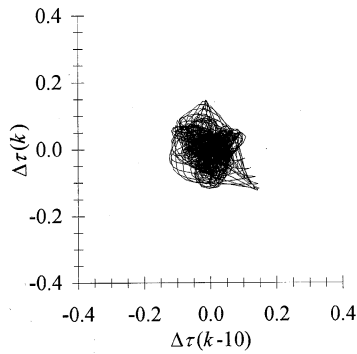


Fig. 19. Three broken bars torque first difference phase space.

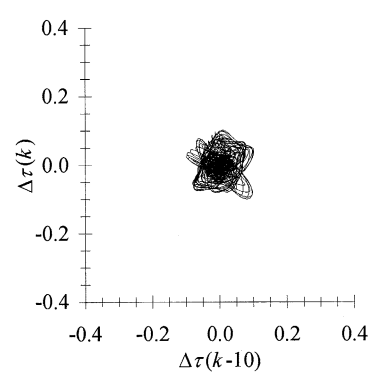


Fig. 23. Six broken connectors torque first difference phase space.

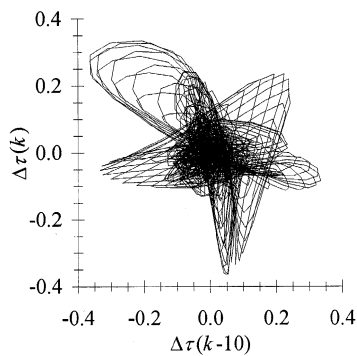


Fig. 20. Six broken bars torque first difference phase space.

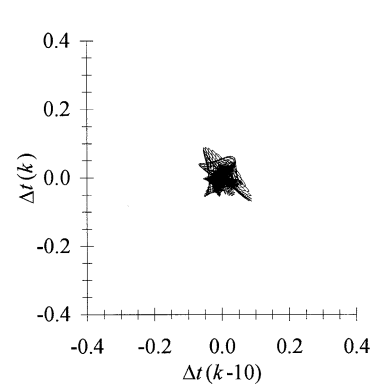


Fig. 24. Nine broken connectors torque first difference phase space.

actual experimental profiles. Although we have not done this with faulty motors, these experimental results have been collected on a healthy version of the motor under several operating conditions [21], [22], [24].

The second concern is the computational requirements needed to generate the simulations. The amount of digital processing, although not trivial, is less demanding than may

TABLE I
RADIUS OF GYRATION FOR TRAINING PHASE SPACES

Operating Mode	Radius of Gyration
Healthy	0.0571
One Broken Bars	0.0892
Three Broken Bars	0.0635
Six Broken Bars	0.1100
Nine Broken Bars	0.0999
Three Broken Connectors	0.0247
Six Broken Connectors	0.0432
Nine Broken Connectors	0.0346
10 % Static Eccentricity	0.0466
30 % Static Eccentricity	0.0480
10 % Dynamic Eccentricity	0.0474
30 % Dynamic Eccentricity	0.0484

TABLE II
STANDARD DEVIATION OF THE RADIUS OF GYRATION FOR TRAINING PHASE SPACES

Operating Mode	Standard Deviation of the Radius of Gyration
10 % Static Eccentricity	0.0648
30 % Static Eccentricity	0.0662
10 % Dynamic Eccentricity	0.0654
30 % Dynamic Eccentricity	0.0663

be expected. An average 4-s simulation takes approximately 36 min on a dual 2-GHz Pentium Xenon processor. All 12 simulations take approximately 7 h if run on a single machine. However, using a standard cluster computing system built on the Condor environment [33], the elapsed time for all simulations may be completed in far less time by running the simulations of the various operating conditions in parallel.

V. RESULTS

From the TSCFE–SS model, we were able to obtain the time-domain simulations for longer time duration than the one-cycle time series shown in Figs. 7–12 for the various torque profiles. Thus, one easily obtains an “out-of-sample” or “test” torque first difference time series for each of the 12 torque profile (torque first difference) cases analyzed by time-delay embedding and radius of gyration calculations. Accordingly, the radius of gyration as a classifying feature was confirmed in the “out-of-sample” or “test” version of each motor mode of operation. The results are shown in Tables I and II for the sample simulations, and all compare well on a one-to-one correspondence with the out-of-sample values given in Tables III and IV, for each case by case, respectively. For example, the sample or training radius of gyration for the healthy motor mode of operation is 0.0571, while the out-of-sample or testing radius of gyration is 0.0585. The sample and out-of-sample radii of gyration for the one broken bar motor mode of operation are 0.0892 and 0.0892, respectively. Likewise, the sample and out-of-sample radii of gyration for the 10% static eccentricity motor mode of operation are 0.0466 and 0.0469, respectively.

The results of the classification algorithm are shown in Tables V–VII. The headings for the tables are as follows: H—Healthy Motor, B1—One Broken Bar, B3—Three Broken Bars, B6—Six Broken Bars, B9—Nine Broken Bars,

TABLE III
RADIUS OF GYRATION FOR TESTING PHASE SPACES

Operating Mode	Radius of Gyration
Healthy	0.0585
One Broken Bars	0.0892
Three Broken Bars	0.0651
Six Broken Bars	0.1108
Nine Broken Bars	0.0994
Three Broken Connectors	0.0272
Six Broken Connectors	0.0441
Nine Broken Connectors	0.0348
10 % Static Eccentricity	0.0469
30 % Static Eccentricity	0.0483
10 % Dynamic Eccentricity	0.0473
30 % Dynamic Eccentricity	0.0487

TABLE IV
STANDARD DEVIATION OF THE RADIUS OF GYRATION FOR TESTING PHASE SPACES

Operating Mode	Standard Deviation of the Radius of Gyration
10 % Static Eccentricity	0.0648
30 % Static Eccentricity	0.0662
10 % Dynamic Eccentricity	0.0653
30 % Dynamic Eccentricity	0.0664

TABLE V
ABSOLUTE DIFFERENCES BETWEEN TRAINING AND TESTING RADII OF GYRATION ($\times 10^{-2}$) PART I

	H	B1	B3	B6	B9	C3
H	0.143	3.069	0.503	5.151	4.136	3.384
B1	0.803	0.002	2.567	2.080	1.066	6.454
B3	5.368	2.409	0.156	4.491	3.477	4.043
B6	4.236	2.157	4.722	0.075	1.089	8.609
B9	2.987	1.025	3.590	1.057	0.043	7.477
C3	0.648	6.199	3.634	8.281	7.267	0.253
C6	2.226	3.859	1.294	5.941	4.927	2.593
C9	1.021	5.437	2.872	7.519	6.505	1.015
S10	0.879	4.232	1.667	6.314	5.300	2.220
S30	0.981	4.090	1.525	6.173	5.158	2.362
D10	0.840	4.193	1.628	6.275	5.261	2.259
D30	0.143	4.051	1.486	6.133	5.119	2.401

TABLE VI
ABSOLUTE DIFFERENCES BETWEEN TRAINING AND TESTING RADII OF GYRATION ($\times 10^{-2}$) PART II

	C6	C9	S10	S30	D10	D30
H	0.861	2.386	1.194	1.053	1.109	1.012
B1	3.932	5.457	4.265	4.124	4.180	4.083
B3	1.521	3.046	1.854	1.713	1.769	1.672
B6	6.086	7.612	6.420	6.279	6.335	6.238
B9	4.954	6.480	5.288	5.147	5.203	5.106
C3	2.269	0.744	1.936	2.077	2.021	2.118
C6	0.070	1.596	0.404	0.263	0.319	0.222
C9	1.508	0.018	1.174	1.315	1.259	1.356
S10	0.303	1.223	0.031	0.110	0.054	0.151
S30	0.161	1.365	0.173	0.031	0.087	0.009
D10	0.263	1.262	0.070	0.071	0.015	0.112
D30	0.122	1.404	0.212	0.071	0.127	0.030

C3—Three Broken Connectors, C6—Six Broken Connectors, C9—Nine Broken Connectors, S10—10% Static Eccentricity,

TABLE VII
ABSOLUTE DIFFERENCES BETWEEN TRAINING AND TESTING STANDARD
DEVIATION OF THE RADII OF GYRATION ($\times 10^{-2}$) PART II

	S10	S30	D10	D30
S10	0.003	0.140	0.057	0.155
S30	0.147	0.004	0.086	0.011
D10	0.052	0.091	0.008	0.106
D30	0.160	0.017	0.100	0.002

S30—30% Static Eccentricity, D10—10% Dynamic Eccentricity, and D30—30% Dynamic Eccentricity. The first column gives the actual mode of operation. The first row indicates the training radius of gyration that was used. The cells of Tables V and VI are the |Training radius of gyration (given by the column heading) – Testing radius of gyration (given by the row heading)|. The minimal difference in each row and, thus, the classification for all but the eccentricity motor modes of operation, is bolded. The cells of Table VII are the |Training standard deviation of the radius of gyration (given by the column heading) – Testing standard deviation of the radius of gyration (given by the row heading)|. The minimal difference in each row and, thus, the classification, is bolded. The results illustrated in Tables V–VII confirm the validity of the approach, because of the small magnitudes of the absolute differences of these bolded radii of gyration and the absolute differences of these standard deviations of radii of gyration, in comparison to all the other differences in the tables (matrices).

We can see in Table VI why a two-step process of classification is required for eccentricity faults. If we use only the radius of gyration, the 30% static eccentricity is misclassified as a 30% dynamic eccentricity. However, as is seen in Table VII, by using the second step and the standard deviation of the radius of gyration, all faults can be correctly classified.

In other words, the classification accuracy on the out-of-sample or testing data is 100%. Beyond the classification accuracy, it is significant to point out that the classifications are robust in the sense that for most of the classifications the next nearest class has absolute difference of radii of gyration that is one to two orders of magnitude greater than the correct class.

VI. LARGE-SCALE IMPLEMENTATION

This proactive approach to fault diagnostics could head off the costly and catastrophic cascading of faults that lead to plant shutdowns and consequent long repair/maintenance periods. The resulting fault identification and diagnostic information also can be used to facilitate the creation of efficient and effective maintenance schedules based on accurate classification of the nature and status of incipient faults associated with a particular motor drive. Future research directions include studying current waveforms, greater numbers of faults, direct comparisons to frequency-based methods, impact of pulswidth-modulation (PWM) control, and various load conditions. Hence, this technique has significant potential in applications to key induction motor ASDs such as in important process industries and similar applications where extended maintenance downtimes cannot be tolerated.

VII. CONCLUSIONS

In conclusion, this paper has presented the integration of the TSCFE–SS method, which can generate a large number of faulty and healthy IMASD simulations, with the TSDM technique, which can automatically characterize and predict IMASD modes of operation. The method was shown to enable one to differentiate between types of faults such as dynamic and static eccentricities and distinguish them from squirrel-cage breakages. The method also distinguishes between the degrees of fault severities such as percentage eccentricities and number of bar as well as connector breakages. Once again, it should be reemphasized that the fault classification achieved by this methodology is robust, in the sense that for most of these fault classifications the next nearest class (other than the fault's calls) has absolute difference of radii of gyration that is one to two orders of magnitude greater than the correct (fault) class. Hence, this dual-track approach could be used to head off the costly and catastrophic cascading of IMASD faults that lead to plant shutdowns and can facilitate the creation of efficient and effective maintenance schedules.

REFERENCES

- [1] M. E. H. Benbouzid, "Bibliography on induction motors faults detection and diagnosis," *IEEE Trans. Energy Conversion*, vol. 14, pp. 1065–1074, Dec. 1999.
- [2] S. J. Manolas and J. A. Tegopoulos, "Analysis of squirrel cage induction motors with broken bars and rings," *IEEE Trans. Energy Conversion*, vol. 14, pp. 1300–1305, Dec. 1999.
- [3] D. G. Dorrell, W. T. Thomson, and S. Roach, "Analysis of airgap flux, current, and vibration signals as a function of the combination of static and dynamic airgap eccentricity in three-phase induction motors," *IEEE Trans. Ind. Applicat.*, vol. 33, pp. 24–34, Jan./Feb. 1997.
- [4] R. F. Walliser and C. F. Landy, "Assessment of interbar currents in double-cage induction motors with broken bars," *IEEE Trans. Energy Conversion*, vol. 9, pp. 159–164, Mar. 1994.
- [5] S. Williamson and K. Mirzoian, "Analysis of cage induction motors with stator winding faults," *IEEE Trans. Power App. Syst.*, vol. PAS-104, pp. 1838–1842, July 1985.
- [6] W. T. Thomson, D. Rankin, and D. G. Dorrell, "On-line current monitoring to diagnose airgap eccentricity—an industrial case history of large hv, three-phase induction motors," *IEEE Trans. Energy Conversion*, pp. 1372–1378, Dec. 1999.
- [7] M. A. Cash, T. G. Habetler, and G. B. Kliman, "Insulation failure prediction in ac machines using line-neutral voltages," *IEEE Trans. Ind. Applicat.*, vol. 34, pp. 1234–1239, Nov./Dec. 1998.
- [8] A. Bethge, P. K. W. Lo, J. T. Phillipson, and J. R. Weldner, "On-line monitoring of partial discharges on stator windings of large rotating machines in the petrochemical environment," *IEEE Trans. Ind. Applicat.*, vol. 34, pp. 1359–1365, Nov./Dec. 1998.
- [9] S. Chen and T. A. Lipo, "Bearing currents and shaft voltages of an induction motor under hard-and soft-switching inverter excitation," *IEEE Trans. Ind. Applicat.*, vol. 34, pp. 1042–1048, Sept./Oct. 1998.
- [10] M. E. H. Benbouzid, H. Nejjar, R. Beguenane, and M. Vieira, "Induction motor asymmetrical faults detection using advanced signal processing techniques," *IEEE Trans. Energy Conversion*, vol. 14, pp. 147–152, June 1999.
- [11] F. Filippetti, G. Franceschini, C. Tassoni, and P. Vas, "AI techniques in induction machines diagnosis including the speed ripple effect," *IEEE Trans. Ind. Applicat.*, vol. 34, pp. 98–108, Jan./Feb. 1998.
- [12] A. J. M. Cardoso, S. M. A. Cruz, and D. S. B. Fonseca, "Inter-turn stator winding fault diagnosis in three-phase induction motors, by Park's vector approach," *IEEE Trans. Energy Conversion*, vol. 14, pp. 595–598, Sept. 1999.
- [13] R. R. Schoen and T. G. Habetler, "Evaluation and implementation of a system to eliminate arbitrary load effects in current-based monitoring of induction machines," *IEEE Trans. Ind. Applicat.*, vol. 33, pp. 1571–1577, Nov./Dec. 1997.
- [14] A. Murray and J. Penman, "Extracting useful higher order features for condition monitoring using artificial neural networks," *IEEE Trans. Signal Processing*, vol. 45, pp. 2821–2828, Nov. 1997.

- [15] G. B. Kliman, W. J. Premerlani, B. Yazici, R. A. Koegl, and J. Mazereeuw, "Sensorless, online motor diagnostics," *IEEE Comput. Applicat. Power*, vol. 10, pp. 39–43, Apr. 1997.
- [16] A. Bernieri, G. Betta, and C. Liguori, "On-line fault detection and diagnosis obtained by implementing neural algorithms on a digital signal processor," *IEEE Trans. Instrum. Meas.*, vol. 45, pp. 894–899, Oct. 1996.
- [17] S. F. Farag, R. G. Bartheld, and T. G. Habetler, "Integrated on-line motor protection system," *IEEE Ind. Applicat. Mag.*, vol. 2, pp. 21–26, Mar./Apr. 1996.
- [18] W. T. Thomson and A. Barbour, "On-line current monitoring and application of a finite element method to predict the level of airgap eccentricity in three-phase induction motors," *IEEE Trans. Energy Conversion*, vol. 13, pp. 347–357, Dec. 1998.
- [19] C.-E. Kim, Y.-B. Jung, S.-B. Yoon, and D.-H. Im, "Fault diagnosis of rotor bars in squirrel cage induction motors by time-stepping finite element method," *IEEE Trans. Magn.*, vol. 33, pp. 2131–2134, Mar. 1997.
- [20] M. J. DeBortoli, S. J. Salon, D. W. Burow, and C. J. Slavik, "Effects of rotor eccentricity and parallel windings on induction machine behavior. A study using finite element analysis," *IEEE Trans. Magn.*, vol. 29, pp. 1676–1682, Mar. 1993.
- [21] J. F. Bangura and N. A. Demerdash, "Performance and torque-ripple characterization in induction motor adjustable speed drives using time-stepping coupled finite element state space techniques," *IEEE Trans. Ind. Applicat.*, vol. 35, pp. 982–990, Sept./Oct. 1999.
- [22] N. A. O. Demerdash and J. F. Bangura, "Characterization of induction motors in adjustable-speed drives using a time-stepping coupled finite-element state-space method including experimental validation," *IEEE Trans. Ind. Applicat.*, vol. 35, pp. 790–802, July/Aug. 1999.
- [23] J. F. Bangura and N. A. Demerdash, "Diagnosis and characterization of effects of broken rotor bars and connectors in squirrel-cage induction motors by a time-stepping coupled finite element-state space modeling approach," *IEEE Trans. Energy Conversion*, vol. 14, pp. 1167–1175, Dec. 1999.
- [24] ———, "Comparison between characterization and diagnosis of broken bars/end-ring connectors and airgap eccentricities of induction motors in asds using a coupled finite element-state space method," *IEEE Trans. Energy Conversion*, vol. 15, pp. 48–56, Mar. 2000.
- [25] ———, "Simulation of inverter-fed induction motor drives with pulse-width modulation by a time-stepping coupled finite element-flux linkage-based state space model," *IEEE Trans. Energy Conversion*, vol. 14, pp. 518–525, Sept. 1999.
- [26] R. J. Povinelli and X. Feng, "Temporal pattern identification of time series data using pattern wavelets and genetic algorithms," in *Proc. Artificial Neural Networks in Engineering*, St. Louis, MO, 1998, pp. 691–696.
- [27] ———, "Data mining of multiple nonstationary time series," in *Proc. Artificial Neural Networks in Engineering*, St. Louis, MO, 1999, pp. 511–516.
- [28] R. J. Povinelli, J. F. Bangura, N. A. O. Demerdash, and R. H. Brown, "Diagnostics of bar and end-ring connector breakage faults in polyphase induction motors through a novel dual track of time-series data mining and time-stepping coupled fe-state space modeling," *IEEE Trans. Energy Conversion*, vol. 17, pp. 39–46, Mar. 2002.
- [29] J. F. Bangura and N. A. O. Demerdash, "Effects of broken bars/end-ring connectors and airgap eccentricities on ohmic and core losses of induction motors in asds using a coupled finite element-state space method," *IEEE Trans. Energy Conversion*, vol. 15, pp. 40–47, Mar. 2000.
- [30] H. D. I. Abarbanel, *Analysis of Observed Chaotic Data*. New York: Springer, 1996.
- [31] F. Takens, "Detecting strange attractors in turbulence," in *Proc. Dynamical Systems and Turbulence*, 1980, pp. 366–381.
- [32] P. A. Tipler, *Physics*, 2nd ed. New York: Worth, 1982, vol. 1.
- [33] (2002) The Condor Project Homepage. [Online] Available: <http://www.cs.wisc.edu/condor/>



John F. Bangura (S'96–M'99) received the B.S.E.E. degree from Clarkson University, Potsdam, NY, in 1994, and the M.S.E.E. and Ph.D. degrees from Marquette University, Milwaukee, WI, in 1996 and 1999, respectively.

He is currently a Senior Engineer with Black & Decker, Baltimore, MD. His research interests include computational electromagnetics applied to electric machines and drives, modeling of dynamic performance of electric machines and drives, as well as condition monitoring and fault diagnosis of

electric machinery drive systems.

Dr. Bangura is a Member of the American Society of Engineering Education and of Sigma Xi.



Richard J. Povinelli (S'85–M'87–SM'01) received the B.S. degree in electrical engineering and the B.A. degree in psychology from the University of Illinois, Champaign-Urbana, in 1987, the M.S. degree in computer and systems engineering from Rensselaer Polytechnic Institute, Troy, NY, in 1989, and the Ph.D. degree in electrical and computer engineering from Marquette University, Milwaukee, WI, in 1999.

From 1987 to 1990, he was a Software Engineer with General Electric Corporate Research and Development. From 1990 to 1994, he was with GE Medical Systems, where he served as a Program Manager and then as a Global Project Leader. From 1995 to 1998, he held the positions of Lecturer and Adjunct Assistant Professor with the Department of Electrical and Computer Engineering, Marquette University, where, since 1999, he has been an Assistant Professor. His research interests include data mining of time series, chaos and dynamical systems, computational intelligence, and financial engineering.

Dr. Povinelli is a Member of the Association for Computing Machinery, American Society of Engineering Education, Tau Beta Pi, Phi Beta Kappa, Sigma Xi, Eta Kappa Nu, Upsilon Pi Epsilon, and Golden Key.



Nabeel A. O. Demerdash (M'65–SM'74–F'90) received the B.Sc.E.E. degree (distinction with first-class honors) from Cairo University, Cairo, Egypt, in 1964, and the M.S.E.E. and Ph.D. degrees from the University of Pittsburgh, Pittsburgh, PA, in 1967 and 1971, respectively.

From 1968 to 1972, he was a Development Engineer with the Large Rotating Apparatus Development Engineering Department, Westinghouse Electric Corporation, East Pittsburgh, PA. From 1972 to 1983, he held the positions of Assistant Professor,

Associate Professor, and Professor in the Department of Electrical Engineering, Virginia Polytechnic Institute and State University, Blacksburg. From 1983 to August 1994, he held the position of Professor in the Department of Electrical and Computer Engineering, Clarkson University, Potsdam, NY. Since 1994, he has been a Professor in the Department of Electrical and Computer Engineering, Marquette University, Milwaukee, WI, in which he served as Department Chair from 1994 to 1997. He is the author or coauthor of more than 100 papers published in various IEEE TRANSACTIONS. His research interests include power electronic applications to electric machines and drives, electromechanical propulsion and actuation, computational electromagnetics in machines and drives, as well as modeling of harmonic effects on machine-power systems dynamics.

Prof. Demerdash is active in the Electric Machinery Committee of the IEEE Power Engineering Society (PES), and its various subcommittees, and is listed in the Distinguished Lecturer Program of the PES and the Distinguished Speaker Program of the IEEE Industrial Electronics Society. He is the winner of the 1999 IEEE Nikola Tesla Technical Field Award. He is also the winner of two 1994 Working Group Awards from both the PES and its Electric Machinery Committee and a winner of two 1993 Prize Paper Awards from both the PES and its Electric Machinery Committee. He is a Member of the American Society of Engineering Education, Sigma Xi, and the Electromagnetics Academy.



Ronald H. Brown (M'72) received the B.S. degree from the University of Illinois, Urbana-Champaign, in 1976, the M.S. degree from the University of Wisconsin, Madison, in 1977, and the Ph.D. degree from The University of Illinois, Urbana-Champaign, in 1986, all in electrical engineering.

He has been on the faculty of Electrical and Computer Engineering at Marquette University, Milwaukee, WI, since 1985. He was with Bell Telephone Laboratories, Indianapolis, IN, and Allen-Bradley Company, Milwaukee, WI, from 1978

to 1982. His research interests include nonlinear system identification, adaptive controls, prediction, and filtering, artificial neural control, and artificial neural network training algorithms.